CHD4 regulates PADI1 and PADI3 expression linking pyruvate kinase M2 citrullination to glycolysis and proliferation.

Sebastien Coassolo[1], Guillaume Davidson[1], Luc Negroni[2], Giovanni Gambi[1], Sylvain Daujat[1], Christophe Romier[3] and Irwin Davidson[1]#.

Institut de Génétique et de Biologie Moléculaire et Cellulaire. CNRS; INSERM; Université de Strasbourg. 1 Rue Laurent Fries, 67404 Illkirch Cedex, France.

1. Department of Functional Genomics and Cancer.

2. Mass-spectrometry platform.

3. Department of Integrated Structural Biology.

FAX: 33 3 88 65 32 01. TEL: 33 3 88 65 34 40 (45)

To whom correspondence should be addressed

E mail : irwin@igbmc.fr

Running Title : Citrullination of PKM2 regulates glycolysis

Key words : NuRD complex, chromatin, melanoma, protein arginine deiminase, allosteric regulation.

The authors declare no potential conflicts of interest.

Abstract.

The CHD4 subunit of the Nucleosome Remodelling and Deacetylation (NuRD) complex regulates expression of PADI1 (Protein Arginine Deiminase 1) and PADI3 in multiple cancer cell types modulating citrullination of three arginines of the allosterically-regulated glycolytic enzyme pyruvate kinase M2 (PKM2). PKM2 citrullination lowers its sensitivity to the inhibitors Tryptophan, Alanine and Phenylalanine shifting the equilibrium towards the activator Serine bypassing normal physiological regulation by low Serine levels and promoting excessive glycolysis, lowered intracellular ATP and slowed proliferation. Our data provide unique insight as to how conversion of arginines to citrulline impacts key interactions within PKM2 adding another layer of complexity to the mechanisms that regulate the activity of this important enzyme.

Results.

CHD3 and CHD4 are mutually exclusive ATPase subunits of the Nucleosome Remodelling and Deacetylation (NuRD) complex that regulates gene expression, acting in many contexts as a co-repressor (*1*) (*2*) (*3*). An shRNA dropout screen previously identified CHD4 as essential for growth of multiple patient derived melanoma xenografts and for breast cancer (*4*) (*5*). Mining public data sets showed up-regulation of CHD4 upon transition from benign nevi to metastatic melanoma (Fig. S1A). In melanomas, CHD4 expression was comparable in the different mutation status, although CHD3 was lowered in NRAS mutated melanomas (Fig. S1B). Single cell RNA-seq (*6*) showed higher CHD4 expression in melanoma tumour cells compared to infiltrating B and T lymphocytes (Fig. S1C). SiRNA-mediated CHD3 or CHD4 silencing in a collection of melanoma cells *in vitro* reduced clonogenic capacity, increased the proportion of slow or non-proliferating cells (Fig. 1A-D), but did not induce apoptosis (Fig. 1E).

RNA-seq following CHD4 silencing in melanoma cells identified more than 1000 up-regulated genes compared to 364 down-regulated genes showing that CHD4 was primarily a transcriptional repressor (Fig. 1F-G, and Dataset S1). In contrast, similar numbers of genes were up or down-regulated by CHD3 silencing (Fig. 1F-G), but no significant overlap of the two genes sets was observed. CHD3 and CHD4 up and down-regulated genes were involved in diverse and distinct sets of pathways (Fig. 1H-I, Dataset S1). De-regulated gene expression was confirmed by RT-qPCR on independent RNA samples in both 501Mel and MM117 melanoma cells (Fig. S2A-B).

Amongst the genes potently up-regulated by CHD4 silencing are *PADI1* (Protein Arginine Deiminase 1) and *PADI3* encoding enzymes that convert arginine to citrulline (*7*)(Fig. S2A-C). In all tested melanoma lines, *PADI3* expression was almost undetectable and potently activated by CHD4 silencing, whereas others had low basal *PADI1* levels that were increased by CHD4 silencing (Fig. S2D). The *PADI1* and *PADI3* genes are located next to each other (Fig. S2E). ChIP-seq in melanoma cells revealed that CHD4 binds together with transcription factors CTCF and FOSL2 (AP1) to an intronic regulatory element in *PADI1* that is predicted to regulate both the *PADI1* and *PADI3* genes (Fig. S3). This element is marked by H2AZ, H3K4me1, BRG1 and ATAC-seq for open chromatin, but not by the lineage-specific transcription factors MITF and SOX10.

To identify potential PADI1/3 substrates in melanoma cells, we made protein extracts from siC and siCHD4 cells, performed immunoprecipitation (IP) with a pan-citrulline antibody and analysed precipitated proteins by mass-spectrometry (Fig. S4A and Dataset S2). An increased number of total peptide spectral matches (PSMs) and PSMs for citrullinated peptides were detected following CHD4 silencing. A set of predominantly cytoplasmic proteins including tubulins, multiple 14-3-3 proteins and glycolytic enzymes PFKP, HK1/2, GAPDH,

ALDOA/C, ENO1/2 and PKM2 were enriched in the IP from siCHD4 cells (Fig. S4B-C and Dataset S2).

We focussed on PKM2, a highly regulated enzyme playing a central role in integrating cellular metabolic status and cell cycle with control of glycolysis (*8*). PKM2 converts phosphoenolpyruvate (PEP) to pyruvate that can then be converted to lactic acid. To investigate PKM2 citrullination by immunoblot following pan-citrulline IP, melanoma cells were transfected with siC, siCHD4 or vectors allowing ectopic expression of PADI1 and PADI3 (Fig. S4D-E). Strongly increased amounts of PKM2 were detected in the IP following siCHD4 compared to siC in both 501Mel and MM117 melanoma cells and after ectopic PADI1 and PADI3 expression, particularly upon co-expression of both enzymes (Fig. S4F-G).

To determine if siCHD4 silencing and the enhanced PKM2 citrullination altered glycolysis, we profiled melanoma cell metabolism in real time. CHD4 silencing in all tested melanoma lines increased the basal OCR (oxygen consumption rate) and ECAR (extracellular acidification rate), markedly increased maximum OCR and ECAR and decreased the OCR/ECAR ratio due to the increased ECAR values (Fig. 2A-D). ECAR was blocked using 2-deoxy-D-glucose confirming that it was due to increased glycolysis (Fig. 2C). Increased glycolysis and lactic acid production diverts pyruvate from oxidative metabolism a more efficient ATP source. Consequently, excessive glycolysis following CHD4 silencing led to decreased intracellular ATP levels (Fig. 2E) at least partially accounting for reduced proliferation.

The increased glycolysis seen upon CHD4 silencing was strongly diminished when *PADI1* and *PADI3* were additionally silenced (Fig. 2F and J). In contrast, exogenous expression of PADI1, PADI3 or both stimulated glycolysis (Fig. 2G and K). Consistent with increased glycolysis, PADI1/3 expression led to reduced intracellular ATP levels (Fig. 2H and L) and

reduced cell proliferation (Fig. 2I). PADI1 and PADI3 were therefore necessary and sufficient for increased glycolysis accounting for the effects seen upon CHD4 silencing.

As mentioned above CHD4 may control PADI1/3 expression not via melanoma-specific factors, but through a regulatory element binding more ubiquitous factors and therefore regulate their expression in non-melanoma cancer cells. SiCHD4 silencing in SiHa cervical carcinoma cells strongly diminished clonogenic capacity (Fig. S5A), potently increased *PADI3* expression (Fig. S5B) and stimulated glycolysis (Fig. S5C-D). Moreover, glycolysis was stimulated by ectopic PADI1/3 expression leading to reduced OCR/ECAR ratio and ATP levels (Fig. S5E-G). In HeLa cells, CHD4 silencing reduced clonogenic capacity and activated *PADI1* and *PADI3* expression (Fig. S5H-I). Glycolysis was stimulated by both CHD4 silencing and ectopic PADI1/3 expression (Fig. S5J). Analogous results were observed in two different types of renal cell carcinoma cell lines (Fig. S5K-T). Therefore, in cell lines from four distinct cancer types, CHD4 silencing or ectopic PADI1/3 expression increased glycolysis and negatively impacted cell proliferation.

In contrast to PKM1 isoform that is constitutively active, PKM2 isoform activity is positively regulated by serine (Ser), fructose 1,6-biphosphate (FBP) and succinylaminoimidazole-carboxamide riboside (SAICAR) and negatively regulated by tryptophan (Trp), alanine (Ala) and phenylalanine (Phe), thus coupling glycolytic flux to the level of critical intermediate metabolites (*9-12*). Allosteric regulation involves three distinct enzyme conformations [(*13-15*) and Figure 3A]. In the apo (resting) state, in absence of small molecules and ions, the PKM2 N-terminal and A domains adopt an active conformation, but the B domain is in an inactive conformation. In the activated R-state, binding of FBP or Ser and magnesium, stabilizes the N and A domains in their active conformation, and rotates the B domain towards the A domain that together form the active site. In the inactive T-state, upon binding of inhibitors (Trp, Ala and Phe), the B domain adopts a partially active conformation,

but the N and A domains undergo structural changes that prevent FBP binding and disorganize the active site. The structural changes observed between the different PKM2 states are reinforced allosterically by organisation into a tetramer that is essential for enzyme function.

In siCHD4 extracts, only 3 citrullinated arginine residues, R106, R246 and R489 were identified by mass-spectrometry and enriched in the siCHD4 extracts (Fig. S4A). R489 is directly involved in FBP binding with interactions between its guanidino group and the FBP 1' phosphate group (Figure 3B). Importantly, despite its extensive interaction network with PKM2, FBP binding is lost upon mutation of R489 into alanine (*13*) (*16*). R489 therefore plays a critical role in FBP binding. Loss of its side chain charge upon citrullination should therefore diminish FBP binding, reinforcing PKM2 allosteric regulation by the free amino acids.

In the apo state, R246 forms salt bridges between its guanidino group and the main chain carboxyl groups of V215 and L217 at the pivotal point where the B domain moves between its active and inactive conformations [(*14*) and Fig. 3C]. This interaction contributes to maintaining the inactive B domain conformation in the apo state and is lost in the R- and T-states. R246 citrullination should strongly weaken or abolish interaction with V215 and L217 facilitating release of the B domain from its inactive conformation.

R106 participates in the free amino acid binding pocket. In the apo state, R106 mostly faces the solvent, but upon free amino acid binding, it rotates towards the pocket and its guanidino group interacts with the carboxylate group of the bound amino acid and the P471 main chain carbonyl [(*9*) (*15*) (*13*) and Fig. 4A]. Ser forms a hydrogen bond network with the N and A domains stabilizing their active conformations, whereas upon Trp, Ala, or Phe binding, their hydrophobic side chain causes displacement of the N-domain outwards leading to the allosteric changes that characterize the inactive T-state (Fig. 4A).

Transition between the R- and T-states is finely regulated by changes in the relative concentrations of Ser versus Trp, Ala and Phe that compete for binding to the pocket (*15*). Loss

of R106 positive side chain charge upon citrullination will weaken its interaction with free amino acids. Due to its extended network of hydrogen bonds within the pocket and as it does not modify the active conformations of the N and A domains, we postulate that Ser binding is less affected, than the hydrophobic amino acids that induce important structural changes within the N and A domains. Consequently, R106 citrullination could weaken the inhibitory effect of Trp, Ala and Phe thereby shifting the equilibrium towards activation by Ser.

To test the above hypotheses, we asked if citrullination modulated glycolysis under different conditions. When cells were grown in absence of Ser, basal glycolysis was reduced and was no longer stimulated upon siCHD4 or PADI1/3 expression (Fig. 4B). On the other hand, exogenous Ser stimulated basal glycolysis that was not further increased by siCHD4 (Fig. 4C). In contrast, basal glycolysis was reduced by exogenous Trp, but remained stimulated by siCHD4 and by PADI1/3 expression (Fig. 4D). Similarly, glycolysis was stimulated by siCHD4 in presence of increasing Phe concentrations (Fig. 4E), an effect particularly visible in MM117 cells where despite strongly inhibited basal glycolysis, stimulation was seen upon siCHD4 (Fig. 4F). PADI1/3 expression also stimulated glycolysis in presence of exogenous Ala (Fig. 4G). PKM2 citrullination did not therefore bypass the requirement for Ser, but diminished inhibition by Trp/Ala/Phe, consistent with the idea that R106 citrullination preferentially diminished binding of Phe, Ala and Trp hence modifying the equilibrium in favour of the activator Ser.

PKM2 is an allostatic regulator integrating a finely balanced feedback mechanism that modulates its activity over a wide range of absolute and relative amino acid concentrations (*15*). When Ser levels are lowered through glycolysis, PKM2 is more readily occupied by inhibitory amino acids reducing glycolysis and allowing accumulation of metabolic intermediates required for Ser synthesis. R106 citrullination upsets this feedback loop by lowering PKM2 sensitivity to Trp/Ala/Phe shifting the equilibrium towards Ser thereby maintaining glycolysis at low Ser concentrations and inhibiting cell proliferation. Previous reports described small

molecules that increase PKM2 activity and stimulate glycolysis resulting in Ser auxotrophy and reduced cell proliferation (*9, 11, 17, 18*). PKM2 citrullination therefore represents a physiological mechanism to regulate glycolysis and cell proliferation adding another layer of complexity to the control of PKM2 activity.

Citrullination of glycolytic enzymes was observed in rheumatoid arthritis (*19*). Tilvawala et al, found that citrullination increased PKM2 enzymatic *in vitro*. We extend these observations to demonstrate that PADI1 and PADI3 citrullinate PKM2 and stimulate glycolysis in cancer cells. Furthermore, our data provide unique insight as to how conversion of arginines to citrulline impacts their key interactions within PKM2 to reprogram its regulation by activating and inhibiting amino acids. While our experiments are consistent with citrullination of PKM2 as the major regulator of glycolysis, PKM2 was not the only glycolytic enzyme that showed increased citrullination and we cannot exclude that their citrullination also contributed to increased glycolysis.

In conclusion, we identify a novel pathway regulating melanoma cell proliferation where CHD4 regulates PADI1 and PADI3 expression and their potential to citrullinate key arginines in PKM2 involved in its allosteric regulation and potentially in other glycolytic enzymes, thereby linking epigenetics to glycolytic flux and cell proliferation. This pathway is shared in other cancer cells indicating a more general mechanism for regulating cell proliferation and a novel potential therapeutic target.

Methods

Cell culture, siRNA silencing and expression vector transfection

Melanoma cell lines 501Mel and SK-Mel-28 were grown in RPMI 1640 medium supplemented with 10% foetal calf serum (FCS). MM074 and MM117 were grown in HAM-

F10 medium supplemented with 10% FCS, 5.2 mM glutamax and 25 mM Hepes. Hermes-3A cell line was grown in RPMI 1640 medium (Sigma) supplemented with 10% FCS, 200nM TPA, 200pM cholera toxin, 10ng/ml human stem cell factor (Invitrogen) and 10 nM endothelin-1 (Bachem). HeLa cells were grown in Dulbecco's modified Eagle's medium supplemented with 10% FCS. SiHA cells were grown in EAGLE medium supplemented with 10% FCS, 0.1mM non-essential amino acids and 1mM sodium pyruvate. UOK cell lines were cultured in DMEM medium (4.5g/L glucose) supplemented with 10% heat-inactivated FCS and 0.1mM AANE.

SiRNA knockdown experiments were performed with the corresponding ON-TARGET-plus SMARTpools purchased from Dharmacon Inc. (Chicago, Il., USA). SiRNAs were transfected using Lipofectamine RNAiMax (Invitrogen, La Jolla, CA, USA) and cells were harvested 72 hours after. PADI1 and PADI3 expression vectors were transfected using X-tremeGENE™ 9 DNA Transfection Reagent (Sigma) for 48h. To assess clonogenic capacity, cells were counted and seeded in 6 well plates for 7 to 15 days.

Proliferation, viability and senescence analyses by flow cytometry

To assess proliferation after siRNA treatment, cells were stained with Cell Trace Violet (Invitrogen) on the day of transfection. To assess cell viability, cells were harvested 72 hours after siRNA transfection and stained with Annexin-V (Biolegend) following manufacturer instructions. To assess senescence, cells were treated with Bafilomycin A (Sigma) for an hour and then with C_{12}FDG (Invitrogen) for two hours. Cells were analysed on a LSRII Fortessa (BD Biosciences) and data were analysed using Flowjo software.

ATP measurement

The concentration of ATP was determined 72h after siRNA transfection using the luminescent ATP detection system (Abcam, ab113849) following the manufacturer's instructions.

Protein extraction and Western blotting

Whole cell extracts were prepared by the standard freeze-thaw technique using LSDB 500 buffer (500 mM KCl, 25 mM Tris at pH 7.9, 10% glycerol (v/v), 0.05% NP-40 (v/v), 16mM DTT, and protease inhibitor cocktail). Cell lysates were subjected to SDS–polyacrylamide gel electrophoresis (SDS-PAGE) and proteins were transferred onto a nitrocellulose membrane. Membranes were incubated with primary antibodies in 5% dry fat milk and 0.01% Tween-20 overnight at 4 °C. The membrane was then incubated with HRP-conjugated secondary antibody (Jackson ImmunoResearch) for 1h at room temperature, and visualized using the ECL detection system (GE Healthcare).

Immunoprecipitation and mass-spectrometry

Citrullinated proteins were immunoprecipitated from whole cell extracts with an anti-pan-citrulline antibody (Abcam, ab6464). Samples were concentrated on Amicon Ultra 0.5 mL columns (cutoff: 10 kDa, Millipore), resolved by SDS-PAGE and stained using the Silver 7 Quest kit (Invitrogen).

Mass spectrometry and analysis

Mass-spectrometry was performed at the IGBMC proteomics platform (Strasbourg, France). Samples were reduced, alkylated and digested with LysC and trypsin at 37°C overnight. Peptides were then analyzed with an nanoLC- MS/MS system (Ultimate nano-LC and LTQ Velos ion trap, Thermo Scientific, San Jose Califronia). Briefly, peptides were separated on a C18 nano-column with a 1 to 30 % linear gradient of acetonitrile and analyzed in a TOP20 CID data-dependent MS method. Peptides were identified with SequestHT algorithm in Proteome Discoverer 2.2 (Thermo Fisher Scientific) *using* Human Swissprot database (20347 sequences). Precursor and fragment mass tolerance were set at 0.9 Da and 0.6 Da respectively. Trypsin was set as enzyme, and up to 2 missed cleavages were allowed. Oxidation (M) and Citrullination (R) were set as variable modifications, and Carbamidomethylation (C) as fixed modification.

Peptides were filtered with a 1 % FDR (false discovery rate) on peptides and proteins. For statistical analyses data was re-analysed using Perseus (*20*).

Chromatin immunoprecipitation and sequencing

CHD4 ChIP experiments were performed on 0.4% Paraformaldehyde fixed and sonicated chromatin isolated from 501Mel cells according to standard protocols as previously described (*21*). MicroPlex Library Preparation kit v2 was used for ChIP-seq library preparation. The libraries were sequenced on Illumina Hiseq 4000 sequencer as Single-Read 50 base reads following Illumina's instructions. Sequenced reads were mapped to the Homo sapiens genome assembly hg19 using Bowtie with the following arguments: -m 1 --strata --best -y -S -l 40 -p 2. After sequencing, peak detection was performed using the MACS software (*22*). Peaks were annotated with Homer (http://homer.salk.edu/homer/ngs/annotation.html) using the GTF from ENSEMBL v75. Peak intersections were computed using bedtools and Global Clustering was done using seqMINER. De novo motif discovery was performed using the MEME suite (meme-suite.org). Motif enrichment analyses were performed using in house algorithms as described in (*23*).

RNA preparation, quantitative PCR and RNA-seq analysis

RNA isolation was performed according to standard procedure (Qiagen kit). qRT-PCR was carried out with SYBR Green I (Qiagen) and Multiscribe Reverse Transcriptase (Invitrogen) and monitored using a LightCycler 480 (Roche). RPLP0 gene expression was used to normalize the results. Primer sequences for each cDNA were designed using Primer3 Software and are available upon request. RNA-seq was performed essentially as previously described (*24*). Gene ontology analyses were performed with the Gene Set Enrichment Analysis software GSEA v3.0 using the hallmark gene sets of the Molecular Signatures Database v6.2 and the functional annotation clustering function of DAVID.

Analysis of oxygen consumption rate (OCR) and glycolytic rate (ECAR) in living cells

The ECAR and OCR were measured in an XF96 extracellular analyzer (Seahorse Bioscience). A total of 20000 cells per well were seeded and transfected by siRNA or expression vector 72h and 24h hours respectively prior the experiment. The cells were incubated in a CO2-free incubator at 37°C and the medium was changed to XF base medium supplemented with 1mM pyruvate, 2 mM glutamine and 10mM glucose for an hour before measurement. For OCR profiling, cells were sequentially exposed to 2 μM oligomycin, 1 μM carbonyl cyanide-4-(trifluorome- thoxy) phenylhydrazone (FCCP), and 0.5 μM rotenone and antimycin A. For ECAR profiling, cells were sequentially exposed to 2 μM oligomycin and 150 mM 2-deoxyglucose (2-DG). After measurement, cells were washed with PBS, fixed with 3% PFA, permeabilized with 0.2% triton. Nuclei were counterstained with Dapi (1:500) and number of cells per well determined by the IGBMC High Throughput Cell-based Screening Facility (HTSF, Strasbourg). L-Phe (Sigma, P2126), L-Trp (Sigma T0254) or L-Ser (Sigma S4500) were added in the complete medium (24-48h for Serine and 6-8h for Trp/Phe) and in the refreshed XF base medium prior the experiment.

Acknowledgements

We thank, Dr Goncalo Castelo-Branco for the PADI3 expression vector, all the staff of the IGBMC common facilities in particular the IGBMC mass spectrometry platform and the high throughput screening facility. This work was supported by institutional grants from the Centre National de la Recherche Scientifique, the Institut National de la Santé et de la Recherche Médicale, the Université de Strasbourg, the Association pour la Recherche contre le Cancer (CR, contract number PJA 20181208268), the Ligue Nationale contre le Cancer, the Institut National du Cancer, the ANR-10-LABX-0030-INRT French state fund through the Agence Nationale de la Recherche under the frame programme Investissements d'Avenir labelled ANR-10-IDEX-0002-02. The IGBMC high throughput sequencing facility is a member of the "France Génomique" consortium (ANR10-INBS-09-08). The mass spectrometry facility is supported by grants from the ARC foundation and from the Canceropole Grand Est. ID is an 'équipe labellisée' of the Ligue Nationale contre le Cancer. SC was supported by a fellowship from the Ligue Nationale contre le Cancer.

Data availability. The CHD4 ChIP-seq and RNA-seq data described here have been deposited in GEO with the accession number GSE134850

Author Contributions

SC performed ChIP-seq, RNA-seq, transfections and metabolism experiments, GD performed bioinformatics analyses, LN performed and analysed mass-spectrometry experiments, GG analysed public data sets, SD constructed and provided PADI1 expression vector, CR performed structural analyses. SC, SD, CR and ID conceived the experiments, analysed the data and wrote the paper.

References.

1. A. P. Bracken, G. L. Brien, C. P. Verrijzer, Dangerous liaisons: interplay between SWI/SNF, NuRD, and Polycomb in chromatin regulation and cancer. *Genes Dev*, (2019).
2. A. Laugesen, K. Helin, Chromatin repressive complexes in stem cells, development, and cancer. *Cell Stem Cell* **14**, 735-751 (2014).
3. P. McDonel, I. Costello, B. Hendrich, Keeping things quiet: roles of NuRD and Sin3 co-repressor complexes during mammalian development. *Int J Biochem Cell Biol* **41**, 108-116 (2009).
4. D. Bossi *et al.*, In Vivo Genetic Screens of Patient-Derived Tumors Revealed Unexpected Frailty of the Transformed Phenotype. *Cancer Discov* **6**, 650-663 (2016).
5. C. D'Alesio *et al.*, RNAi screens identify CHD4 as an essential gene in breast cancer growth. *Oncotarget* **7**, 80901-80915 (2016).
6. I. Tirosh *et al.*, Dissecting the multicellular ecosystem of metastatic melanoma by single-cell RNA-seq. *Science* **352**, 189-196 (2016).
7. K. L. Bicker, P. R. Thompson, The protein arginine deiminases: Structure, function, inhibition, and disease. *Biopolymers* **99**, 155-163 (2013).
8. Z. Lu, T. Hunter, Metabolic Kinases Moonlighting as Protein Kinases. *Trends Biochem Sci* **43**, 301-310 (2018).
9. B. Chaneton *et al.*, Serine is a natural ligand and allosteric activator of pyruvate kinase M2. *Nature* **491**, 458-462 (2012).
10. H. R. Christofk *et al.*, The M2 splice isoform of pyruvate kinase is important for cancer metabolism and tumour growth. *Nature* **452**, 230-233 (2008).
11. T. L. Dayton, T. Jacks, M. G. Vander Heiden, PKM2, cancer metabolism, and the road ahead. *EMBO Rep* **17**, 1721-1730 (2016).
12. K. E. Keller, I. S. Tan, Y. S. Lee, SAICAR stimulates pyruvate kinase isoform M2 and promotes cancer cell survival in glucose-limited conditions. *Science* **338**, 1069-1072 (2012).
13. H. P. Morgan *et al.*, M2 pyruvate kinase provides a mechanism for nutrient sensing and regulation of cell proliferation. *Proc Natl Acad Sci U S A* **110**, 5881-5886 (2013).
14. J. D. Dombrauckas, B. D. Santarsiero, A. D. Mesecar, Structural basis for tumor pyruvate kinase M2 allosteric regulation and catalysis. *Biochemistry* **44**, 9417-9429 (2005).
15. M. Yuan *et al.*, An allostatic mechanism for M2 pyruvate kinase as an amino-acid sensor. *Biochem J* **475**, 1821-1837 (2018).
16. J. A. Macpherson *et al.*, Functional cross-talk between allosteric effects of activating and inhibiting ligands underlies PKM2 regulation. *Elife* **8**, (2019).
17. D. Anastasiou *et al.*, Pyruvate kinase M2 activators promote tetramer formation and suppress tumorigenesis. *Nat Chem Biol* **8**, 839-847 (2012).
18. C. Kung *et al.*, Small molecule activation of PKM2 in cancer cells induces serine auxotrophy. *Chem Biol* **19**, 1187-1198 (2012).
19. R. Tilvawala *et al.*, The Rheumatoid Arthritis-Associated Citrullinome. *Cell Chem Biol* **25**, 691-704 e696 (2018).
20. S. Tyanova *et al.*, The Perseus computational platform for comprehensive analysis of (prote)omics data. *Nat Methods* **13**, 731-740 (2016).
21. P. Laurette *et al.*, Transcription factor MITF and remodeller BRG1 define chromatin organisation at regulatory elements in melanoma cells. . *eLife* **10.7554/eLife.06857**, (2015).
22. Y. Zhang *et al.*, Model-based analysis of ChIP-Seq (MACS). *Genome Biol* **9**, R137 (2008).

23. S. Joshi *et al*., TEAD transcription factors are required for normal primary myoblast differentiation in vitro and muscle regeneration in vivo. *PLoS Genet* **13**, e1006600 (2017).
24. P. Laurette *et al*., Chromatin remodellers Brg1 and Bptf are required for normal gene expression and progression of oncogenic Braf-driven mouse melanoma. *Cell Death Differ*, (2019).
25. T. Strub *et al*., Essential role of microphthalmia transcription factor for DNA replication, mitosis and genomic stability in melanoma. *Oncogene* **30**, 2319-2332 (2011).

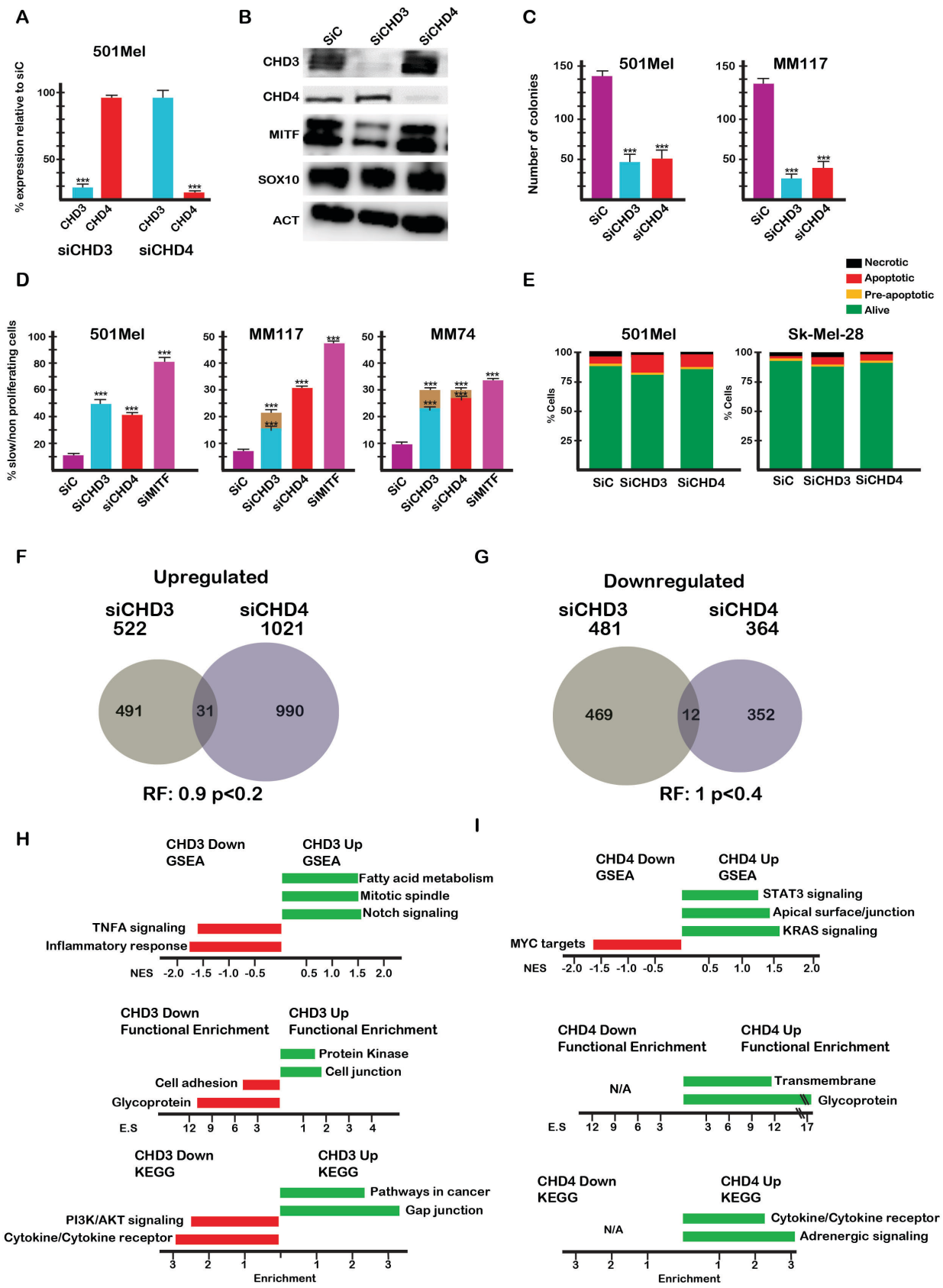

Coassolo et al., Figure 1

Figure 1. CHD3 and CHD4 are required for normal melanoma cell proliferation. **A-B**. 501Mel cells were transfected with the indicated siRNAs and CHD3 and CHD4 expression evaluated by RT-qPCR or by immunoblot along with that of MITF and SOX10. **C**. The indicated cell lines were transfected with siRNA and after reseeding the number of colonies counted after 10 days. **D**. The indicated cell lines were transfected with siRNAs and cell proliferation evaluated by cell trace violet assay. **E**. The indicated cell lines were transfected with siRNA and apoptosis detected by FACs after labelling with Annexin-V. In all experiments N=3 and unpaired t-tests analyses were performed by Prism 5. P-values: *= p<0,05; **= p<0,01; ***= p<0,001. Silencing of MITF known to induce cell cycle arrest and senescence was included as a control (*25*). **F-G** RNA-seq was performed on triplicate samples of 501Mel cells after transfection of siRNA. Genes up or down-regulated based on Log2 fold-change >1/<-1 with an adjusted p-value <0,05 were identified. Venn diagrams show overlap between the CHD3 and CHD4 regulated genes along with the hypergeometric probability representation factor (RF), in this case non-significant. **I-H**. Ontology analyses of CHD3 and CHD4 regulated genes. Shown are the enrichment scores for GSEA, as well as David functional enrichment and KEGG pathway categories.

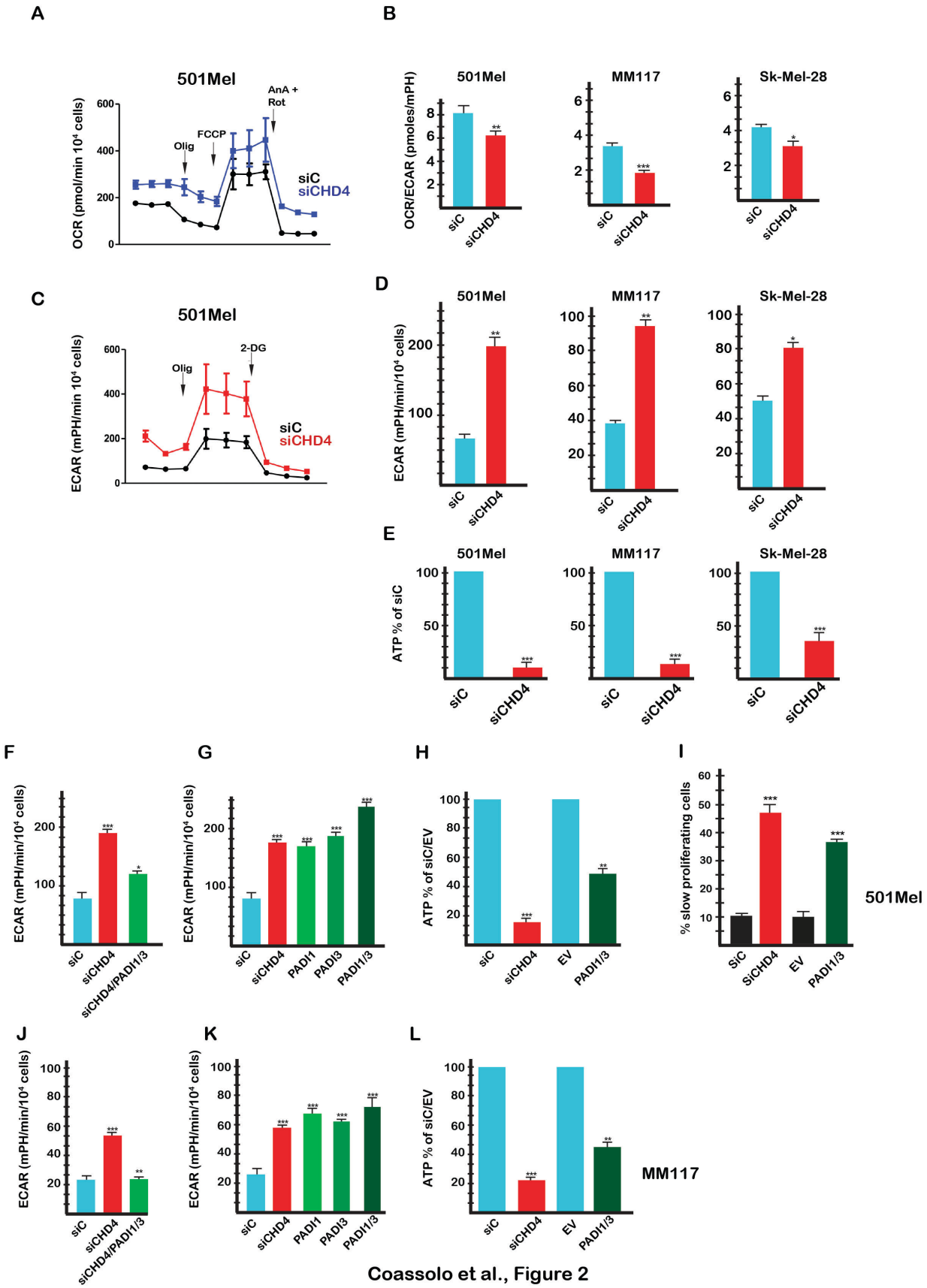

Coassolo et al., Figure 2

Figure 2. CHD4 silencing regulates glycolysis and cell proliferation. **A.** Effect of CHD4 silencing on basal and maximal OCR values in 501Mel cells. **B**. Effect of CHD4 silencing on the basal OCR/ECAR ratio in the indicated cell types. **C-D**. Effect of CHD4 silencing on basal and maximal ECAR values in 501Mel cells and basal ECAR values in the indicated cell types. **E.** CHD4 silencing reduces intracellular ATP levels in the indicated cell lines. **F-G**. ECAR values in 501Mel cells following transfection with indicated siRNAs or expression vectors. **H.** Intracellular ATP levels following CHD4 silencing or PADI1/3 expression. EV = empty expression vector control. **I** Reduced cell proliferation following PAD1/3 expression. **J-L**. ECAR values and intracellular ATP levels in MM117 cells following transfection with indicated siRNAs or expression vectors. In all experiments ECAR values were determined from N=6 with 6 technical replicates for each N. Unpaired t-test analyses were performed by Prism. P-values: *= p<0,05; **= p<0,01; ***= p<0,001.

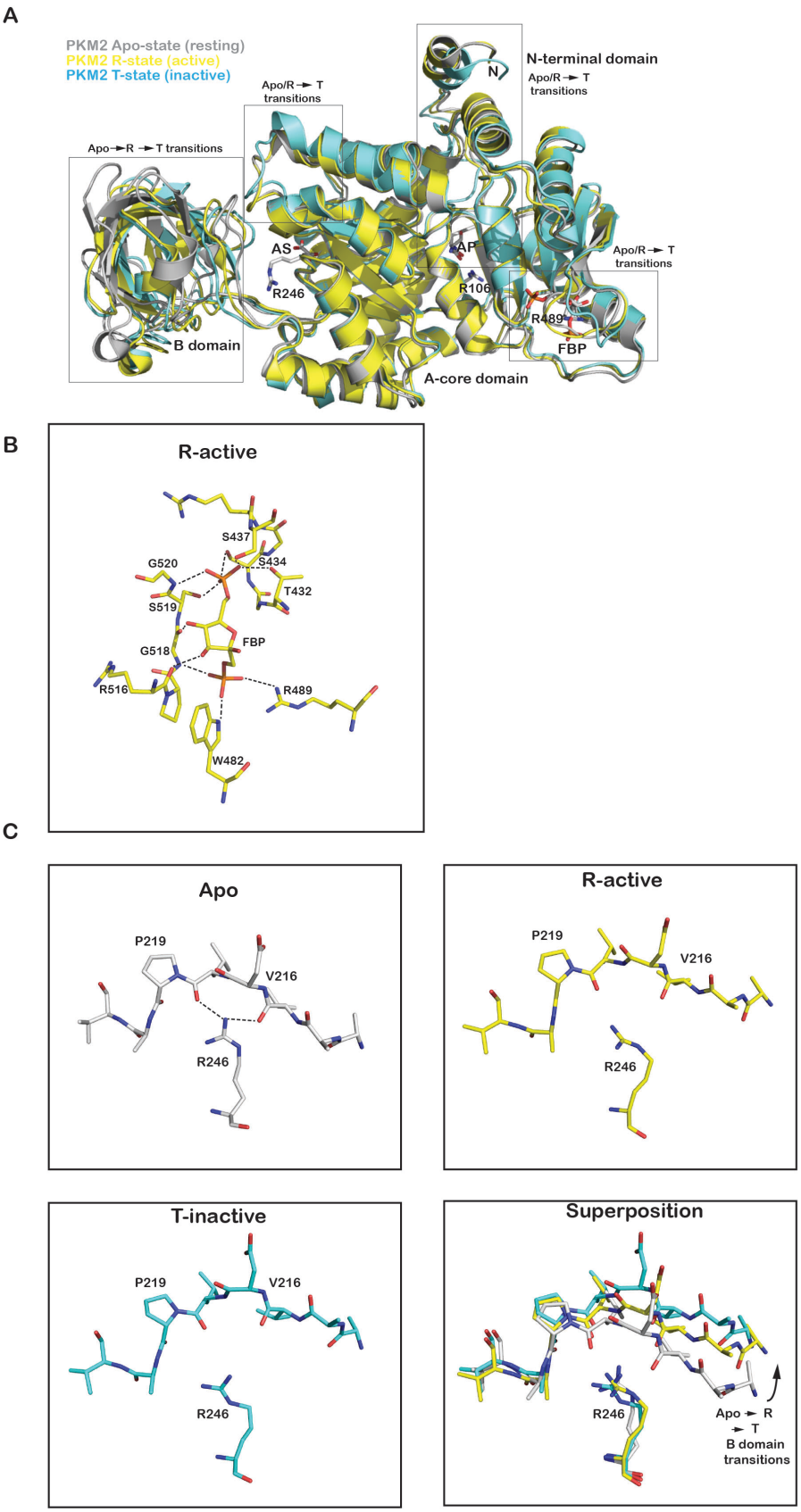

Coassolo et al., Figure 3

Figure 3. Locations and interactions of citrullinated arginines in PKM2. **A.** Ribbon representation of a PKM2 monomer in the apo resting state (grey; PDB 3SRH), the active R state (yellow; PDB 6GG6 with FBP and oxalate molecules from 3SRD) and the inactive T state (cyan; PDB 6GG4). The three citrullinated arginines (R106, R246 and R489), the free amino acids Serine and Phenylalanine, FBP and oxalate (surrogate of pyruvate to occupy the active site) are shown as sticks (carbon, grey; nitrogen, blue; oxygen, red; phosphorus, orange). AS, active site. AP, free amino acid binding pocket. The regions of PKM2 undergoing allosteric structural transitions between the three states are boxed. **B.** Close up view of FBP interactions within the R-active state. Salt bridges and hydrogen bonds are shown as dashed lines. Colour coding as panel A. For clarity, the side chain of K433 is not displayed. **C.** Closeup view of R246 interactions with the B domain in the Apo, R-active and T-inactive states along with a superposition of the three structures. Colour coding and representation of salt bridges/hydrogen bonds is as in panels A and B.

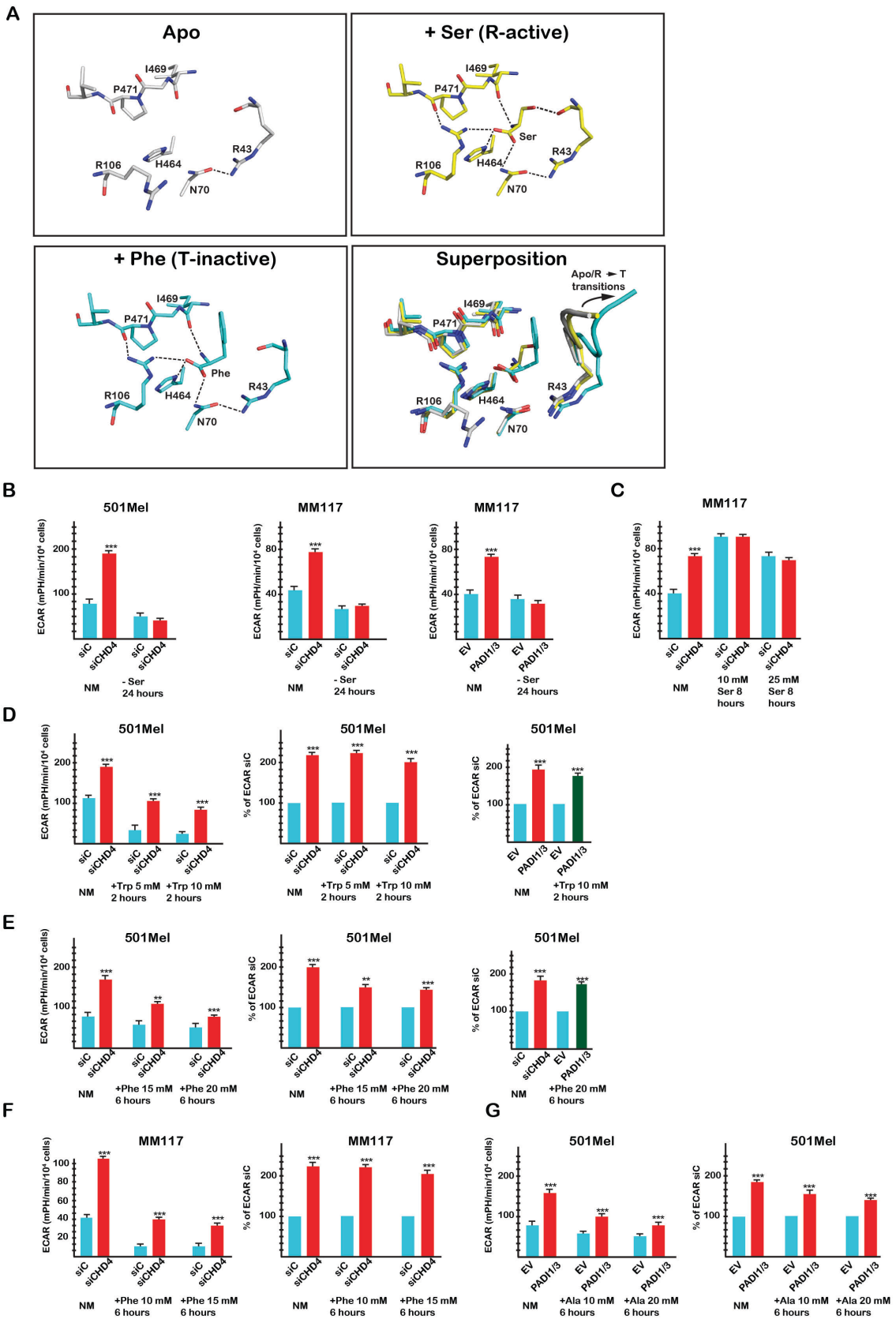

Coassolo et al., Figure 4

Figure 4. PKM2 citrullination diminishes allosteric inhibition by Phe/Ala/Trp. **A.** Close up view of free Ser and Phe interactions within the free amino acid binding pocket in the Apo, R-active and T-inactive states with a superposition of the three structures. All residues displayed are shown as sticks. In the superposition, the peptide bearing R43 is represented as ribbon to show the allosteric changes created upon Phe binding. Colour coding is as in Fig. 3. Salt bridges and hydrogen bonds are shown as dashed lines. For clarity, the side chain of Phe 470, which stacks on R106 side chain, is not displayed. **B**. ECAR values in presence of exogenous Ser or absence of Ser after CHD4 silencing or PADI1/3 expression in 501Mel or MM117 cells; NM = normal medium. **C.** ECAR values in presence of increased exogenous Ser with or without CHD4 silencing in 501Mel cells. **D-E**. ECAR values in presence of exogenous Trp or Phe with or without CHD4 silencing or PADI1/3 expression in 501Mel cells. **F**. ECAR values in presence of exogenous Phe with or without CHD4 silencing in MM117 cells. **G.** ECAR values in presence of exogenous Ala with or without PADI1/3 expression in 501Mel cells. In all experiments ECAR values were determined from N=6 with 6 technical replicates for each N. Unpaired t-test analysis were performed by Prism 5. P-values: *= p<0,05; **= p<0,01; ***= p<0,001.